International Journal of Nanomedicine

Dovepress
Taylor & Francis Group

Open Access Full Text Article

ORIGINAL RESEARCH

Thermosensitive in situ Hydrogel Based on Benzalkonium Chloride-Loaded Selenium-Doped Mesoporous Silica Nanoparticles for Diabetic Chronic Wound Treatment

Yukun Liu[1,*], Kang Wang[1,*], Yuanyuan Li[2], Keyan Lv[2], Mengran Yang[2], Zhanfei Li[3–6], Xiangjun Bai[3–6], Fangli Gao[2], Yuchang Wang[3–6]

[1]Department of Plastic and Aesthetic Surgery, Tongji Hospital, Tongji Medical College, Huazhong University of Science and Technology, Wuhan, 430030, People's Republic of China; [2]College of Chemistry and Chemical Engineering, Henan Normal University, Xinxiang, 4453007, People's Republic of China; [3]Division of Trauma Surgery, Emergency Surgery & Surgical Critical Care, Tongji Hospital, Tongji Medical College, Huazhong University of Science and Technology, Wuhan, 430030, People's Republic of China; [4]Sino-German Research Institute of Disaster Medicine, Huazhong University of Science and Technology, Wuhan, 430030, People's Republic of China; [5]Department of Emergency and Critical Care Medicine, Tongji Hospital, Tongji Medical College, Huazhong University of Science and Technology, Wuhan, 430030, People's Republic of China; [6]Trauma Center, Tongji Hospital, Tongji Medical College, Huazhong University of Science and Technology, Wuhan, 430030, People's Republic of China

*These authors contributed equally to this work

Correspondence: Fangli Gao; Yuchang Wang, Email 13312191217@126.com; tjwangyuchang@tjh.tjmu.edu.cn

Background: Diabetic chronic wounds are characterized by persistent infection, excessive oxidative stress, impaired angiogenesis, and prolonged inflammation, resulting in delayed healing. Current wound dressings lack the ability to simultaneously regulate these pathological processes.

Methods: A multifunctional composite hydrogel was developed by incorporating benzalkonium chloride (BAC)-loaded selenium-doped mesoporous silica nanoparticles (Se-MSNs) into a PF127 matrix. In this system, BAC provides antibacterial activity, Se-MSNs enable redox regulation and immunomodulation, and PF127 serves as a delivery platform for localized retention and sustained release. The physicochemical properties, antibacterial activity, antioxidant capacity, pro-angiogenic effects, and anti-inflammatory performance were evaluated in vitro, followed by therapeutic assessment in a diabetic mouse wound model.

Results: The composite hydrogel exhibited effective antibacterial activity against Staphylococcus aureus and Escherichia coli, reduced intracellular reactive oxygen species, promoted endothelial cell migration and tube formation, and modulated inflammatory cytokine expression in vitro. In vivo, the hydrogel significantly accelerated wound closure, enhanced collagen deposition and angiogenesis, and alleviated excessive inflammation in diabetic wounds.

Conclusion: The therapeutic effects of the composite hydrogel are attributed to the restoration of redox homeostasis and the coordinated regulation of inflammation resolution and vascular regeneration. This study presents a multifunctional biomaterial strategy for improving the healing of diabetic chronic wounds.

Keywords: selenium-doped mesoporous silica, thermosensitive hydrogel, benzalkonium chloride, diabetic wound, antibacterial, pro-angiogenesis

Introduction

Diabetic chronic wounds represent one of the most challenging complications of diabetes, often arising from persistent inflammation, impaired angiogenesis, elevated oxidative stress, and recurrent infections.[1–3] These factors collectively extend the inflammatory phase and hinder the progression toward tissue regeneration, frequently resulting in wounds that are slow to heal or prone to recurrence.[4,5] Despite the development of various pharmacological therapies, their clinical use is often limited by high costs, variable therapeutic outcomes, and logistical challenges.[6–8] As a result, conventional

https://doi.org/10.2147/IJN.S594500
Received: 3 February 2026
Accepted: 10 May 2026
Published: 23 May 2026

Graphical Abstract

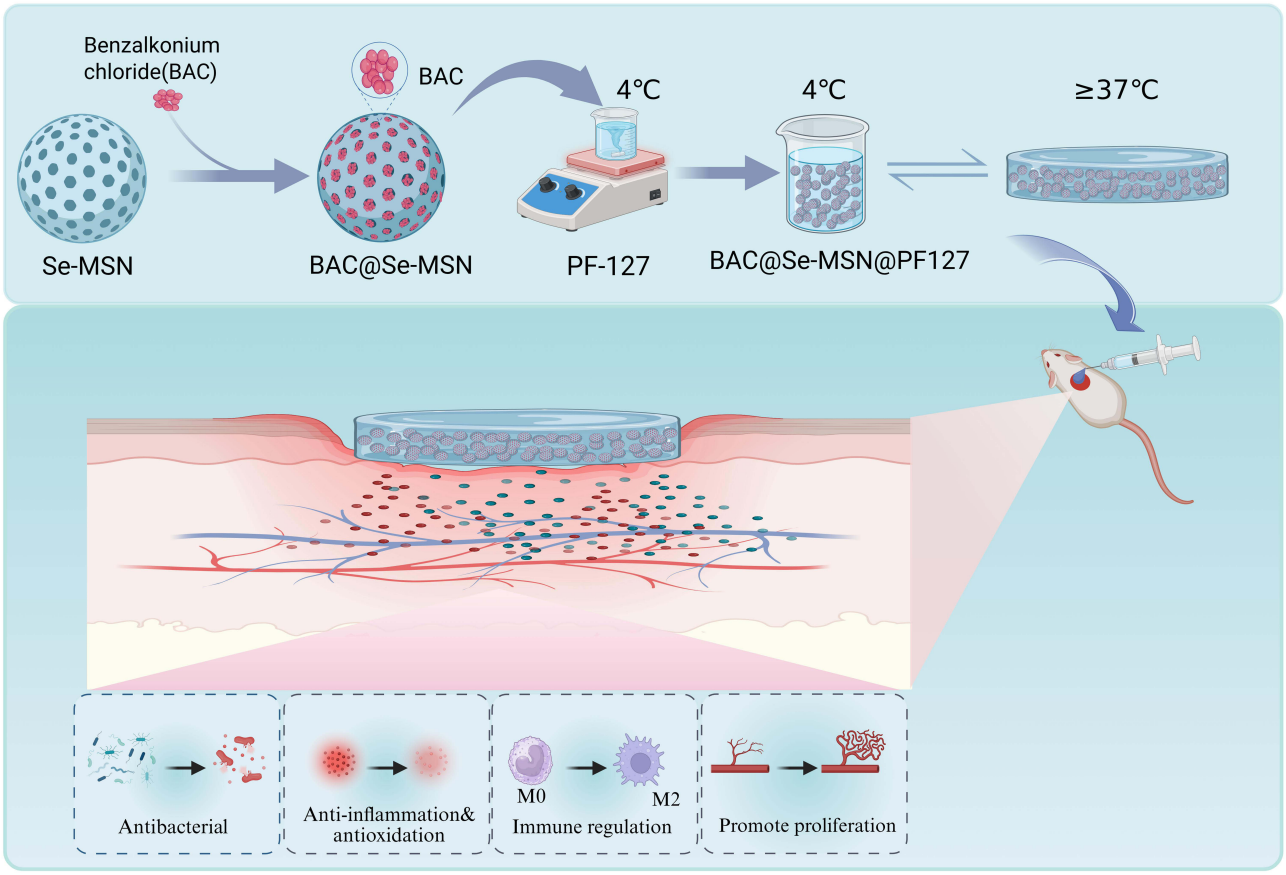

approaches—such as repeated debridement, skin grafting, infection management, and standard dressing care—remain the primary treatment strategies, yet they often fall short in effectively resolving chronic, non-healing wounds.[9]

Bacterial infection is a prominent factor leading to the worsening and delayed healing of diabetic wounds.[10–12] Traditional antibiotic therapy generally fails due to bacterial resistance and biofilm protection.[13–15] Benzalkonium chloride (BAC), a quaternary ammonium cationic surfactant, demonstrates broad-spectrum antibacterial activity by breaking bacterial membranes and reducing biofilm formation, while also being appropriate for large-scale production and cost-effective.[14,16] However, direct application of BAC is limited by high toxicity, fast release, and local discomfort. Loading BAC into nanocarriers can enable sustained release and lower toxicity, balancing safety and antibacterial efficacy.[17–19]

In recent years, nanotechnology-based smart biomaterials have presented new potential for chronic wound therapy.[20,21] Among these, mesoporous silica nanoparticles (MSNs) have been widely employed in drug administration and tissue healing due to their huge surface area, variable pore size, simple functionalization, and outstanding biocompatibility.[22–24] However, traditional MSNs function solely as passive carriers, lacking inherent bioactivity and the ability to actively alter the wound microenvironment. To solve this constraint, researchers have integrated functional elements into their structure to bestow bioresponsive capabilities. Selenium (Se), an essential trace element, has a key role in maintaining cellular redox homeostasis, scavenging reactive oxygen species (ROS), and modulating immunological responses.[25,26] Incorporating selenium into the mesoporous silica network endows the material with prolonged antioxidant and anti-inflammatory activity, presenting a unique method to alleviate oxidative stress in chronic wounds.[27,28] In addition to effective carrier design, local retention and drug delivery efficiency are significant factors

of therapeutic success. Thermosensitive hydrogels, with their injectability and reversible sol–gel transition, have emerged as suitable platforms for wound-targeted drug delivery.[29] Pluronic F127 (PF127), an FDA-approved thermosensitive block copolymer, remains fluid at low temperature but rapidly gels at body temperature, enabling in situ gelation and prolonged release of medicines at the wound site.[30]

In recent years, multifunctional smart hydrogel dressings have attracted widespread attention as a novel platform for wound repair. Several studies have developed composite hydrogels that simultaneously possess antibacterial, antioxidant, anti-inflammatory, and tissue-regenerative properties, such as plant-derived antibacterial-prioritized designs[31] and functional bioactive hydrogel systems.[32] These works provide important inspiration for the multi-functional synergistic strategy employed in the present study; however, most of these systems still exhibit limitations in the coordinated regulation of inflammation and angiogenesis. Therefore, in this work, we integrated antibacterial (BAC), antioxidant and immunomodulatory (Se-MSNs), and controlled-release (PF127) functionalities into a single composite platform, aiming to achieve more comprehensive regulation of the wound microenvironment.

Our previous study reported a rosuvastatin-loaded periodic mesoporous organosilica (PMO) –gold nanostar-based hydrogel that promoted diabetic wound healing mainly through modulation of inflammatory responses and cytoskeletal remodeling via the cGMP–PKG and RhoA–MLCK–MLC pathways.[33] In this work, we engineered a thermoresponsive composite hydrogel (BAC@Se-MSNs/PF127) designed to coordinate antibacterial, antioxidant, and immune-modulating functions for comprehensive regulation of the diabetic wound milieu. Within this system, selenium-modified mesoporous silica nanoparticles (Se-MSNs) act as the functional backbone, offering sustained redox protection and immunoregulatory support. BAC is incorporated to deliver potent, broad-spectrum antimicrobial activity, while PF127 provides temperature-dependent injectability and controlled drug release. The formulation remains in a flowable state at low temperatures, enabling uniform coverage of complex wound geometries, and undergoes rapid gelation at physiological temperatures to maintain prolonged local retention and therapeutic action. This multifunctional platform introduces a versatile material strategy and conceptual basis for advancing nano-polymer composite therapies in chronic diabetic wound management.

Materials and Methods

Materials and Reagents

Selenium powder, sodium borohydride ($NaBH_4$), tetraethyl orthosilicate (TEOS), 3-aminopropyltriethoxysilane, and 3-chloropropyltriethoxysilane were obtained from Aladdin. Fetal bovine serum (FBS) was purchased from Hyclone, and DMEM, RPMI-1640, and trypsin were sourced from Gibco. All aqueous solutions were prepared using double-distilled water (DDW).

Male BALB/c mice (8 weeks old) were supplied by the Animal Center of Tongji Hospital, Tongji Medical College, Huazhong University of Science and Technology. This animal experiment was approved by the Animal Management and Use Committee of Tongji Hospital, Huazhong University of Science and Technology (approval number: T1-202505014, Wuhan, China).

Synthesis of Se-MSNs and BAC Loading

Se-MSNs were synthesized following a sol–gel route. The diselenide-functionalized silane precursor bis[3-(triethoxysilyl)propyl]diselenide (BTESePD) was generated according to a previously described method[11]. A mixture of TEOS and BTESePD was dissolved in anhydrous ethanol and gradually transferred into a CTAT/triethanolamine solution under continuous stirring at 80 °C for 4 h. The molar ratio and synthesis conditions were selected based on previously reported protocols with slight modifications to ensure structural stability and reproducibility. The resulting solid was isolated by centrifugation, washed with ethanol, and collected as a light-yellow powder.

To remove the CTAT template, the powder was dispersed in methanol containing ammonium nitrate (2% w/v) and refluxed for 3 h at 80°C. After cooling, the suspension was centrifuged and rinsed with ethanol. The extraction was repeated twice, and the purified nanoparticles were stored in ethanol. For drug loading, Se-MSNs were sonicated in deionized water for 10 min and then incubated with BAC solution under light-protected stirring for 24 h. BAC-loaded Se-MSNs were collected by centrifugation, washed repeatedly to eliminate free BAC, and vacuum-dried. Due to the

focus of this study on the overall biological performance of the composite hydrogel, the drug loading capacity and encapsulation efficiency of BAC were not quantitatively determined, and loading was primarily confirmed by UV–vis spectroscopy and zeta potential analysis.

Characterization of BAC@Se-MSNs

Nanoparticle morphology and dimension were evaluated using transmission electron microscopy (TEM, JEOL). Elemental mapping (Si, O, Se, N, Cl) was conducted with TEM-EDS. Surface charge was assessed using a Zetasizer Nano ZS (Malvern). UV–vis spectra (200–400 nm, Shimadzu) were recorded to verify the presence of BAC on Se-MSNs.

Preparation and Characterization of BAC@Se-MSNs/PF127 Thermosensitive Composite Hydrogel

BAC@Se-MSNs were added to the PF127 solution at a final concentration of XX mg/mL unless otherwise specified. The mixture remained flowable at low temperature and transformed into a semi-solid gel at 37 °C. Chemical interactions among PF127, Se-MSNs, and the hybrid hydrogel were examined via FTIR (Thermo Nicolet). SEM imaging was carried out to assess microstructural organization and pore morphology. For release studies, a defined amount of hydrogel was immersed in PBS (pH 7.4) at 37°C. Samples were taken at set intervals, and BAC content in the supernatant was quantified by UV–vis spectroscopy. Rheological behaviors (frequency and strain sweeps) were measured using a Discovery HR-3 rheometer (TA Instruments). As PF127 is a physically crosslinked thermosensitive hydrogel, its structural disintegration in aqueous environments mainly occurs through gradual dissolution rather than chemical degradation.

Cell Culture

HUVECs, NIH-3T3 fibroblasts, and RAW264.7 macrophages were purchased from ATCC. All cell lines were maintained in DMEM supplemented with 10% FBS and 1% penicillin–streptomycin under 5% CO_2 at 37 °C.

Cell Viability and Survival Assays

Cells were treated with different concentrations of the tested materials. Viability on days 1, 3, and 5 was quantified using the CCK-8 kit (Dojindo). After adding 10 μL reagent per well and incubating for 2 h, absorbance was measured at 450 nm.

Live/dead status was visualized after 48 h exposure using Calcein-AM/PI staining (Invitrogen) and observed via fluorescence microscopy.

Evaluation of Antioxidant Activity

Oxidative stress in HUVECs was induced using H_2O_2, followed by treatment with various concentrations of BAC@Se-MSNs/PF127. Cell viability was assessed with CCK-8.DPPH assays (Solarbio) were used to evaluate free radical scavenging activities by incubating hydrogel samples with DPPH solution in the dark for 30 min and measuring absorbance at 517 nm.

Intracellular ROS levels were determined using DCFH-DA (Beyotime). After staining and incubation for 30 min, fluorescence intensity was analyzed by microscopy and a microplate reader.

Inflammatory Cytokine Expression Analysis

Supernatants were collected, and levels of IL-6, TNF-α, and IL-10 were quantified with ELISA kits (Servicebio). Absorbance was detected at 450 nm, and cytokine concentrations were interpolated from standard curves and normalized for comparison.

Scratch Wound Healing Assay

HUVEC monolayers in 6-well plates were scratched using a sterile pipette tip. Cells were then incubated with various extraction solutions, with or without NIR exposure. Images were captured at 0, 12, and 24 h, and migration efficiency was calculated as:

$$\text{Scratch Healing}(\%) = \frac{S_0 - S_t}{S_0} \times 100\%$$

Where S_0 represents the initial scratch area and S_t represents the scratch area at the given time.

Tube Formation Assay

Matrigel-coated 96-well plates (50 μL/well) were polymerized at 37°C for 30 min. HUVECs (2×10^4 cells/well) were seeded with different treatment media (Control, PF127, BAC@PF127, Se-MSNs@PF127, BAC@Se-MSNs/PF127; 1.0 mg/mL). Tube-like structures were imaged, and network parameters (nodes, tube length) were quantified using ImageJ's Angiogenesis Analyzer.

In vitro Antibacterial Evaluation

Plate counting assays were conducted using *E. coli* (ATCC 25922) and *S. aureus* (ATCC 29213). Bacterial suspensions (1×10^3 CFU/mL) were plated, and treatment samples were placed centrally. After 6 h incubation, bacterial solutions were serially diluted, re-plated, and cultured for 24 h at 37°C for CFU assessment.

SYTO9/PI staining was used to visualize live/dead bacteria (green/red). Growth kinetics were measured by incubating ~10^6 CFU/mL suspensions in a microplate reader at 37°C with shaking; OD_{600} was recorded every 2 h for 24 h to generate growth curves.

Establishment of Diabetic Mouse Model and Wound Analysis

Male C57BL/6 mice (8 weeks, 20–25 g) were acclimated for one week. Diabetes was induced by intraperitoneal Streptozotocin (STZ) injection (50 mg/kg in 0.1 M citrate buffer, pH 4.5) for five consecutive days. Mice displaying fasting glucose ≥16.7 mmol/L twice were considered diabetic.

Under anesthesia, dorsal hair was removed, and a circular full-thickness wound (10 mm) was created. Animals were randomized into five groups (n=5): Control, PF127, BAC/PF127, Se-MSNs/PF127, and BAC@Se-MSNs/PF127. Dressings were replaced daily. Wounds were photographed on days 0, 3, 5, 7, 10, and 14.

$$\text{Wound healing rate}(\%) = \frac{A_0 - A_t}{A_0} \times 100\%$$

where A_0 represents the initial wound area and A_t represents the wound area at a specific time. This animal experiment was approved by the Animal Management and Use Committee of Tongji Hospital, Huazhong University of Science and Technology (approval number: T1-202505014, Wuhan, China).

Histological and Immunohistochemical Analysis

Animals were euthanized at predetermined time points. Wound tissues were fixed in 4% paraformaldehyde, embedded in paraffin, and sectioned (5 μm).

H&E staining assessed tissue morphology, while Masson's trichrome evaluated collagen production. IHC was performed for CD31 and Ki67 (DAB visualization).

Immunofluorescence staining for CD68, CD206, and iNOS was carried out, and five random regions per section were quantified using ImageJ.

RNA Sequencing and Transcriptome Analysis

Wound samples (day 7, n = 3 per group) were snap-frozen in liquid nitrogen. RNA extraction was performed using TRIzol, and RNA quantity/quality was checked via Nanodrop and Agilent Bioanalyzer. Libraries were constructed and

sequenced on an Illumina HiSeq X10 platform. Bioinformatic analysis was carried out using NovoMagic (Novogene) and Majorbio.

Statistical Analysis

All experiments were replicated at least three times. Data are expressed as mean ± SD. Statistical comparisons were conducted using Student's *t*-test or one-way ANOVA followed by Tukey's test (GraphPad Prism 9). $P < 0.05$ was considered statistically significant.

Results and Discussion

Synthesis and Characterization of BAC@Se-MSNs Nanocomposites

To obtain a nanosystem capable of simultaneously providing antibacterial and antioxidant functions, selenium-modified mesoporous silica nanoparticles (Se-MSNs) were fabricated via a sol–gel process and subsequently loaded with benzalkonium chloride (BAC). The preparation workflow is summarized in Figure 1A. TEM imaging verified that the as-prepared Se-MSNs possessed a well-defined spherical morphology with uniform dispersion and an average size near 50 nm, together with evident mesoporous surfaces (Figure 1B and C). Elemental mapping by EDS demonstrated evenly distributed Si, O, and Se signals, while the appearance of N and Cl indicated successful BAC incorporation (Figures 1B and S1). In this system, selenium is incorporated into the silica framework through organosilane precursors, likely existing in the form of Se–Se or related covalent bonds rather than as discrete selenium nanoparticles. Although the Se signal intensity appears relatively low, it is uniformly distributed within the silica framework, indicating successful incorporation at a trace yet functional level.

Zeta potential analysis further confirmed the surface modification: pristine Se-MSNs exhibited a mildly positive potential (7.9 mV), which markedly increased to 32.9 mV after BAC loading (Figure 1D), reflecting the cationic nature of BAC and its strong surface association. UV–vis spectroscopy of the BAC@Se-MSNs/PF127 mixture showed a characteristic absorption feature around ~280 nm, although the peak appeared relatively broad due to the composite nature of the system (Figure 1E). This may be attributed to the overlapping absorption and scattering effects from the polymer matrix and silica framework.

In addition, the reduced absorbance intensity of BAC in the supernatant after loading suggests that a substantial proportion of BAC was successfully incorporated into the Se-MSNs, indicating a relatively high loading efficiency.

Preparation and Characterization of BAC@Se-MSNs/PF127 Thermosensitive Hydrogel

To enhance localized retention and achieve controlled drug release, BAC@Se-MSNs were dispersed into Pluronic F127, forming a thermosensitive hydrogel system (Figure 2A). The formulation remained in a low-viscosity state at 4°C, while heating to physiological temperature triggered rapid sol–gel transition, producing a semi-solid matrix (Figure 2B). This rapid sol–gel transition enables the hydrogel to form a stable covering layer at the wound site, contributing to localized retention and sustained drug release.

FTIR spectra provided further evidence for successful hybrid formation (Figure 2C). PF127 displayed typical C–H stretching vibrations (2880–2970 cm^{-1}) and a strong C–O–C band at 1100 cm^{-1}, whereas Se-MSNs exhibited Si–O–Si vibrations at ~1080, 800, and 460 cm^{-1} and a Si–OH signal near 950 cm^{-1}. The composite hydrogel showed intensified Si–O–Si bands accompanied by slight wavelength shifts, suggesting interfacial interactions—likely hydrogen bonding—between the polymer chains and the inorganic framework.

SEM images confirmed that both pure PF127 and the composite hydrogel possessed interconnected porous architectures characteristic of thermosensitive polymer networks (Figure 2D). Drug-release assays showed a gradual and sustained release of BAC over 72 h, demonstrating the hydrogel's capacity to regulate drug diffusion (Figure 2E). This sustained release behavior also indirectly reflects the gradual structural disintegration of the hydrogel in aqueous conditions.

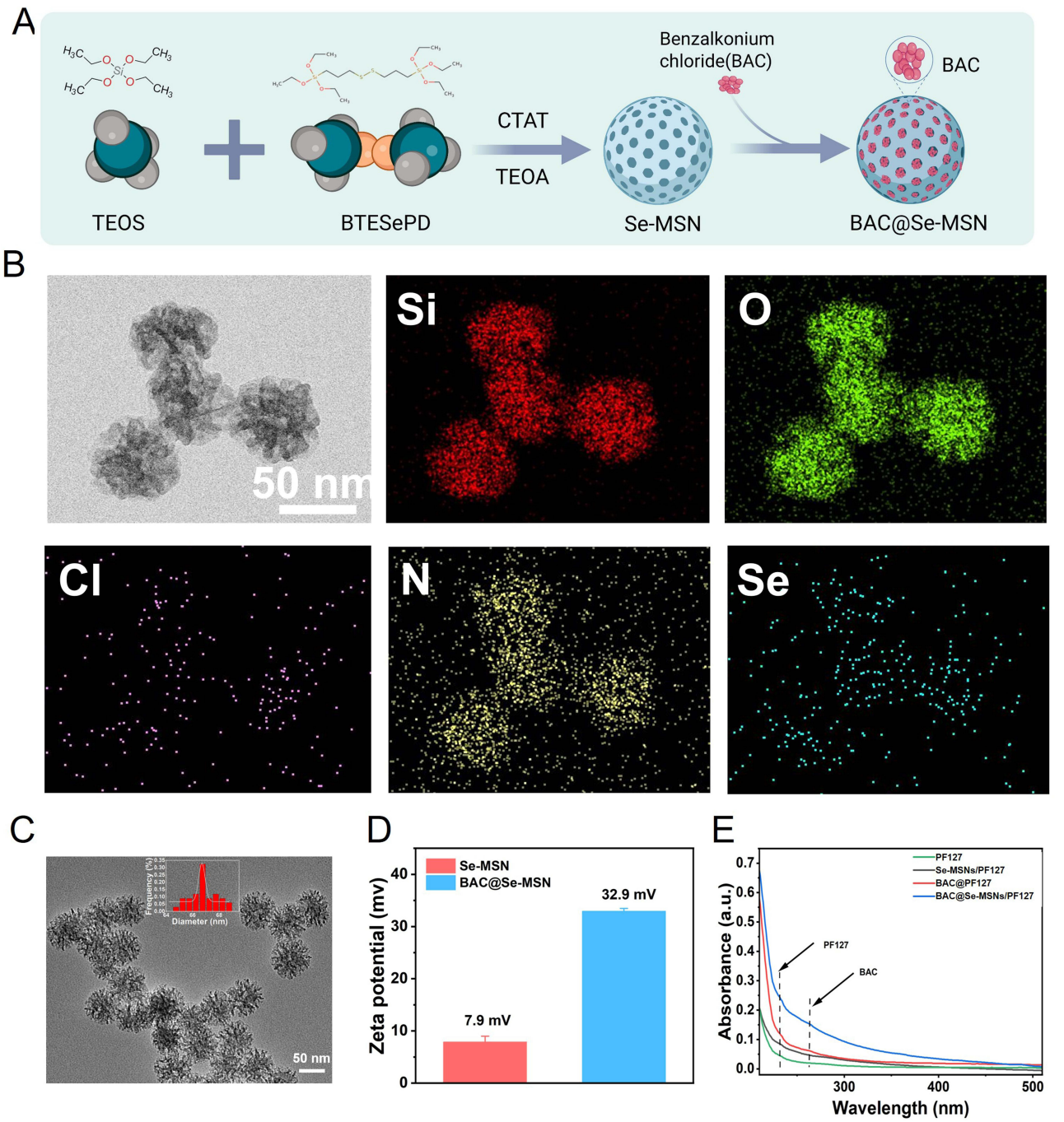

Figure 1 Preparation and characterization of BAC@Se-MSNs nanocomposites. (**A**) Schematic representation of BAC@Se-MSNs synthesis: Se-containing mesoporous silica nanoparticles (Se-MSNs) were synthesized utilizing TEOS and BTSePD in a CTAT/TEOA system, followed by loading benzalkonium chloride (BAC) to generate BAC@Se-MSNs. (**B**) TEM pictures and EDS elemental mapping revealing uniform distribution of Si, O, Se, N, and Cl, suggesting successful BAC loading. (**C**) TEM picture revealing consistent spherical morphology of BAC@Se-MSNs with an average diameter of ~50 nm. (**D**) Zeta potential measurement: Se-MSNs and BAC@Se-MSNs displayed surface potentials of 7.9 mV and 32.9 mV, respectively. (**E**) UV–Vis spectra of BAC@Se-MSNs/PF127 displaying characteristic BAC absorption peak at 280 nm, suggesting effective incorporation. The characteristic absorption peaks of BAC and PF127 are marked by dashed lines.

Rheological measurements indicated that G′ consistently exceeded G″ in amplitude sweeps, and both parameters remained stable under time and frequency sweeps (Figure 2F–H), reflecting robust elasticity, structural integrity, and reliable viscoelastic performance. Such thermosensitive hydrogels can achieve effective local retention through rapid in situ gelation at physiological temperature, without relying on strong tissue adhesion. It should be noted that the present hydrogel system is not specifically engineered for strong tissue adhesion. Instead, its local retention primarily depends on

https://doi.org/10.2147/IJN.S594500

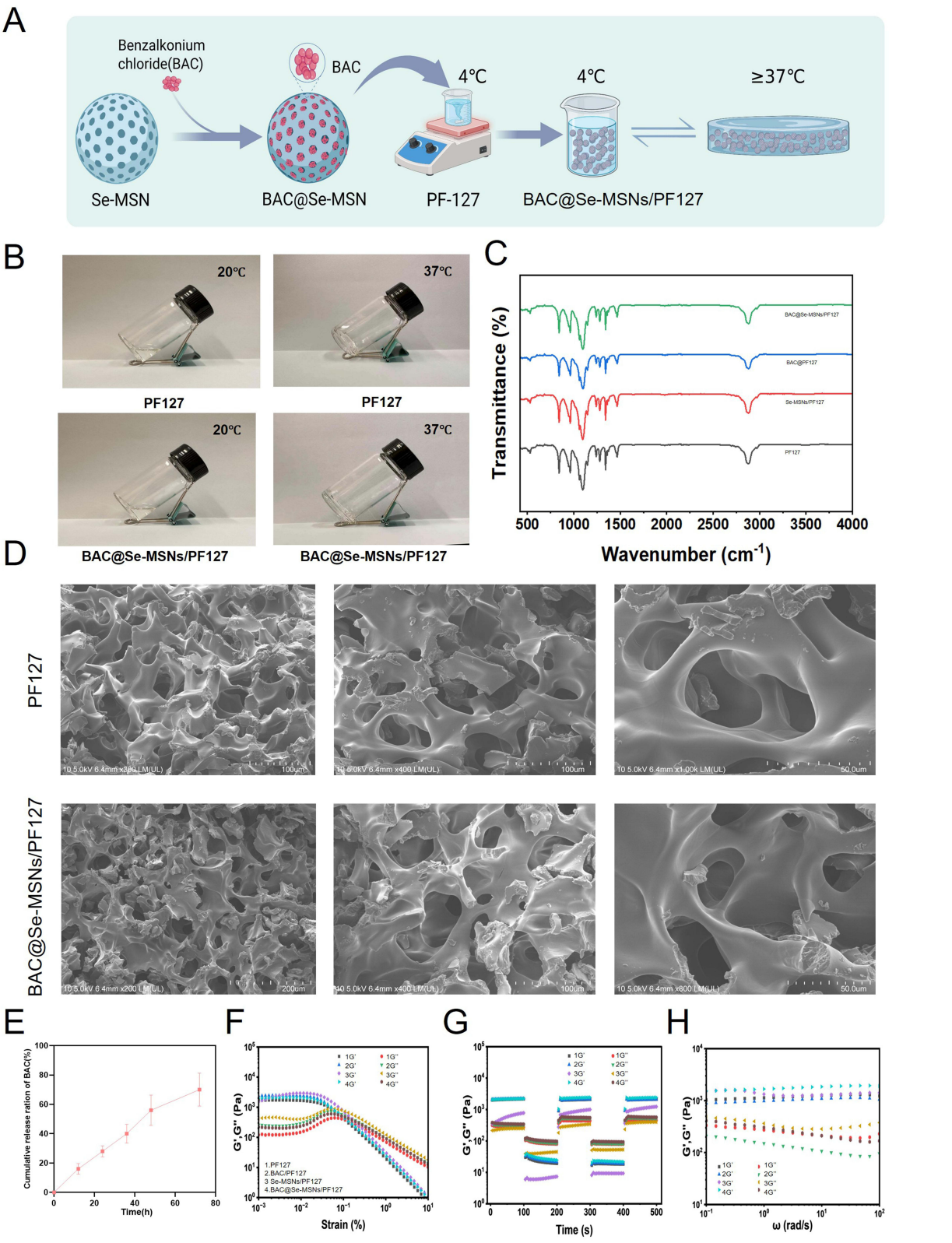

Figure 2 Preparation and structural characterisation of BAC@Se-MSNs/PF127 thermosensitive hydrogel. (**A**) Schematic depiction of hydrogel preparation: BAC-loaded Se-MSNs were combined with PF127 solution at 4°C, followed by gelation at 37°C. (**B**) Photographs illustrating temperature-responsive behavior: PF127 and BAC@Se-MSNs /PF127 were liquid at 20°C and formed stable gels at 37°C. (**C**) FTIR spectra exhibiting typical peaks of PF127, Se-MSNs, and BAC, suggesting successful composite production. FTIR spectra are provided for qualitative assessment of surface functional groups; peak overlap may obscure some minor signals. (**D**) SEM images exhibiting porous structures in PF127 and BAC@Se-MSNs/PF127 hydrogels. (**E**) Cumulative release profile of BAC from BAC@Se-MSNs/PF127, exhibiting persistent release behavior. (**F**–**H**) Rheological analysis: amplitude scan (F), time sweep (G), and frequency sweep (**H**) showing G′ > G″, indicating good viscoelasticity and structural stability.

https://doi.org/10.2147/IJN.S594500

temperature-triggered in situ gelation. While this mechanism is sufficient for maintaining coverage and enabling sustained drug release in relatively static wound environments, it may be less effective in highly dynamic conditions. Future work will focus on incorporating adhesive functional groups to further enhance tissue integration and retention.

Biocompatibility, Antioxidant, and Anti-Inflammatory Effects of BAC@Se-MSNs/PF127 Hydrogel

The biological safety and functional properties of BAC@Se-MSNs/PF127 were assessed using HUVECs and NIH-3T3 cells. CCK-8 data revealed that the composite exhibited negligible cytotoxicity at 0.5–1.0 mg/mL over 5 days, whereas a higher concentration (2.0 mg/mL) mildly inhibited proliferation (Figure 3A and B). Therefore, 1.0 mg/mL was selected for subsequent experiments. Live/Dead staining further confirmed high cell viability, with predominantly green fluorescence after 48 h of treatment (Figure 3C). Additional dose-response experiments (5–40 μg/mL) showed viability consistently above 90% (Figure S2).

In diabetic wounds, excessive production of reactive oxygen species (ROS) due to mitochondrial dysfunction creates sustained oxidative pressure, which subsequently amplifies pro-inflammatory cascades—particularly NF-κB activation—leading to chronic inflammation and impaired repair.[34–37] Selenium is known to participate in enzymatic antioxidant defense (eg, GPx family) and thus contributes to redox homeostasis.[38] In an H_2O_2-induced oxidative injury model, cells treated with the BAC@Se-MSNs/PF127 hydrogel showed substantially higher viability (Figure 3D). The material also demonstrated effective free-radical scavenging in DPPH assays (Figure 3E) and significantly lowered intracellular ROS levels, as visualized using DCFH-DA staining (Figure 3F). Furthermore, inflammatory cytokine profiling indicated that the hydrogel markedly reduced IL-6 and TNF-α while elevating the anti-inflammatory cytokine IL-10 (Figure 3G–I). The antioxidant and anti-inflammatory effects are mainly attributed to the incorporation of selenium within the silica framework, which can participate in redox regulation and mimic the activity of endogenous selenoproteins. Upon gradual release or surface interaction, selenium species contribute to the scavenging of reactive oxygen species and modulation of inflammatory signaling pathways.

BAC@Se-MSNs Hydrogel Promotes Endothelial Cell Migration and Angiogenesis

Because impaired angiogenesis is a major pathological barrier in diabetic wound repair, the pro-angiogenic potential of the composite hydrogel was examined.[39] In scratch assays, HUVECs treated with BAC@Se-MSNs/PF127 exhibited significantly accelerated wound closure at both 12 and 24 h compared with Control, PF127, and BAC@PF127 groups (Figure 4A–D, $P < 0.001$). Notably, the effect was comparable to that of the Se-MSNs@PF127 group, highlighting the dominant contribution of selenium-based nanoparticles to endothelial motility.

Tube formation assays further demonstrated enhanced angiogenic behavior (Figure 4B, E and F). Previous studies have demonstrated that selenium-based materials can promote endothelial cell migration and angiogenesis by regulating oxidative stress and related signaling pathways.[38,40] The composite hydrogel promoted the formation of longer and more interconnected tubular networks, including increased numbers of nodes and total tube length. PF127 and BAC@PF127, in contrast, showed minimal angiogenic improvement relative to the control. These results indicate that Se-MSNs serve as the major pro-angiogenic component, and the full composite system robustly supports vascular regeneration processes relevant to chronic diabetic wound healing.

BAC@Se-MSNs Hydrogel Exhibits Excellent Antibacterial Activity

Chronic diabetic wounds are frequently complicated by persistent bacterial colonization and biofilm development, which hinder repair and aggravate inflammation.[10,41,42] Given the known bactericidal properties of BAC-containing systems, the antibacterial capabilities of the composite hydrogel were systematically evaluated. Plate culture assays demonstrated that PF127 and Se-MSNs@PF127 alone provided limited antibacterial activity, whereas hydrogels containing BAC substantially decreased colony formation, with BAC@Se-MSNs/PF127 showing the most pronounced suppression (Figure 5A). SYTO9/PI staining validated these results at the single-cell level: both *E. coli* and *S. aureus* exhibited

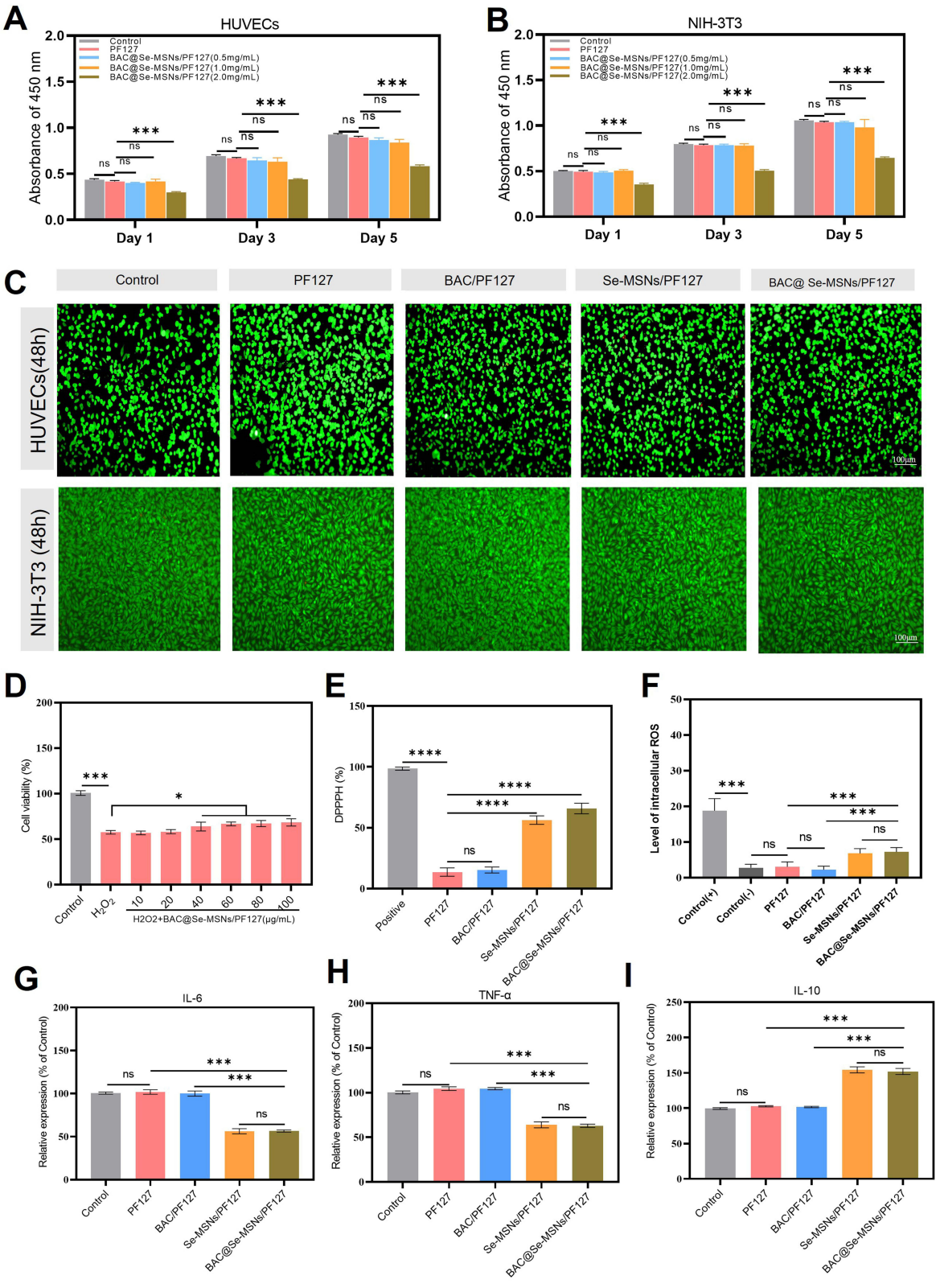

Figure 3 Biocompatibility, antioxidant, and anti-inflammatory effects of BAC@Se-MSNs/PF127 hydrogel in vitro. (**A** and **B**) CCK-8 assay showing viability of HUVECs (**A**) and NIH-3T3 cells (**B**) after 1, 3, and 5 days under different treatments (Control, PF127, BAC@Se-MSNs/PF127 at 0.5, 1.0, 2.0 mg/mL). (**C**) Live/Dead staining shows great cell viability (green) in all groups, exhibiting strong biocompatibility. (**D**) Cell survival after H_2O_2-induced oxidative damage, exhibiting considerable protection by BAC@Se-MSNs/PF127. (**E**) DPPH radical scavenging experiment revealing significant antioxidant activity of BAC@Se-MSNs/PF127. (**F**) Intracellular ROS levels demonstrating effective decrease by BAC@Se-MSNs/PF127. (**G–I**) RT-qPCR investigation revealing downregulation of pro-inflammatory factors IL-6 (**G**) and TNF-α (**H**) and overexpression of anti-inflammatory IL-10 (**I**) in BAC@Se-MSNs/PF127-treated cells. Data are shown as mean ± SD; *P < 0.05, ***P < 0.001, ****P < 0.0001, ns, not significant.

https://doi.org/10.2147/IJN.S594500

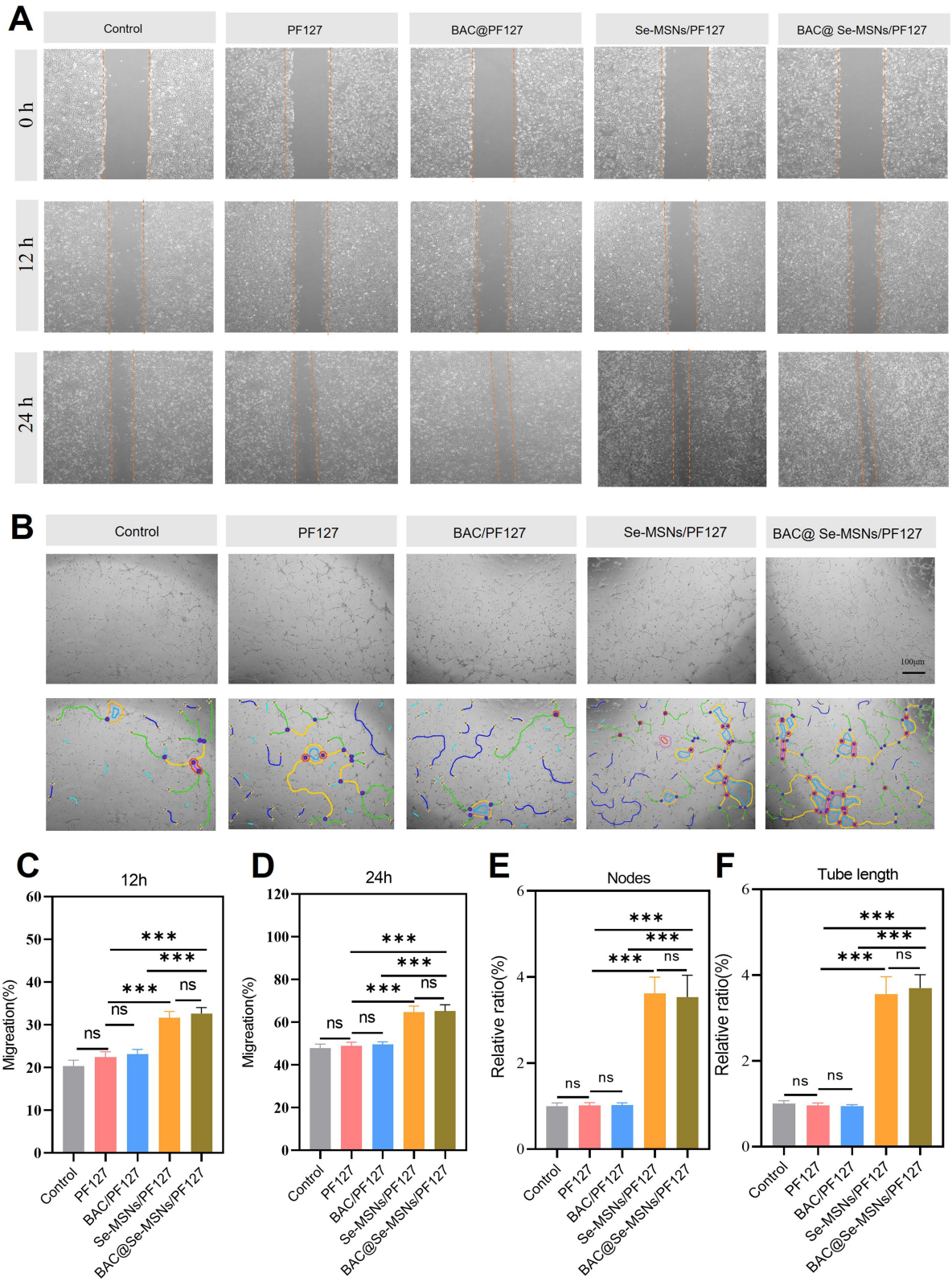

Figure 4 BAC@Se-MSNs/PF127 hydrogel promotes HUVEC migration and in vitro angiogenesis. (**A**) Representative photos of scratch wound assay at 0, 12, and 24 h for different treatments (Control, PF127, BAC@PF127, Se-MSNs@PF127, BAC@Se-MSNs/PF127). (**B**) Tube formation assay images and quantitative analysis.(**C**) Quantification of HUVEC migration at 12 h. (**D**) Quantification of HUVEC migration at 24 h. (**E**) Relative measurement of nodes in the tube formation experiment. (**F**) Relative measurement of tube lengths in the tube formation experiment. Data are mean ± SD (n = 3); ***P < 0.001, ns, not significant. Scale bar = 100 μm.

https://doi.org/10.2147/IJN.S594500

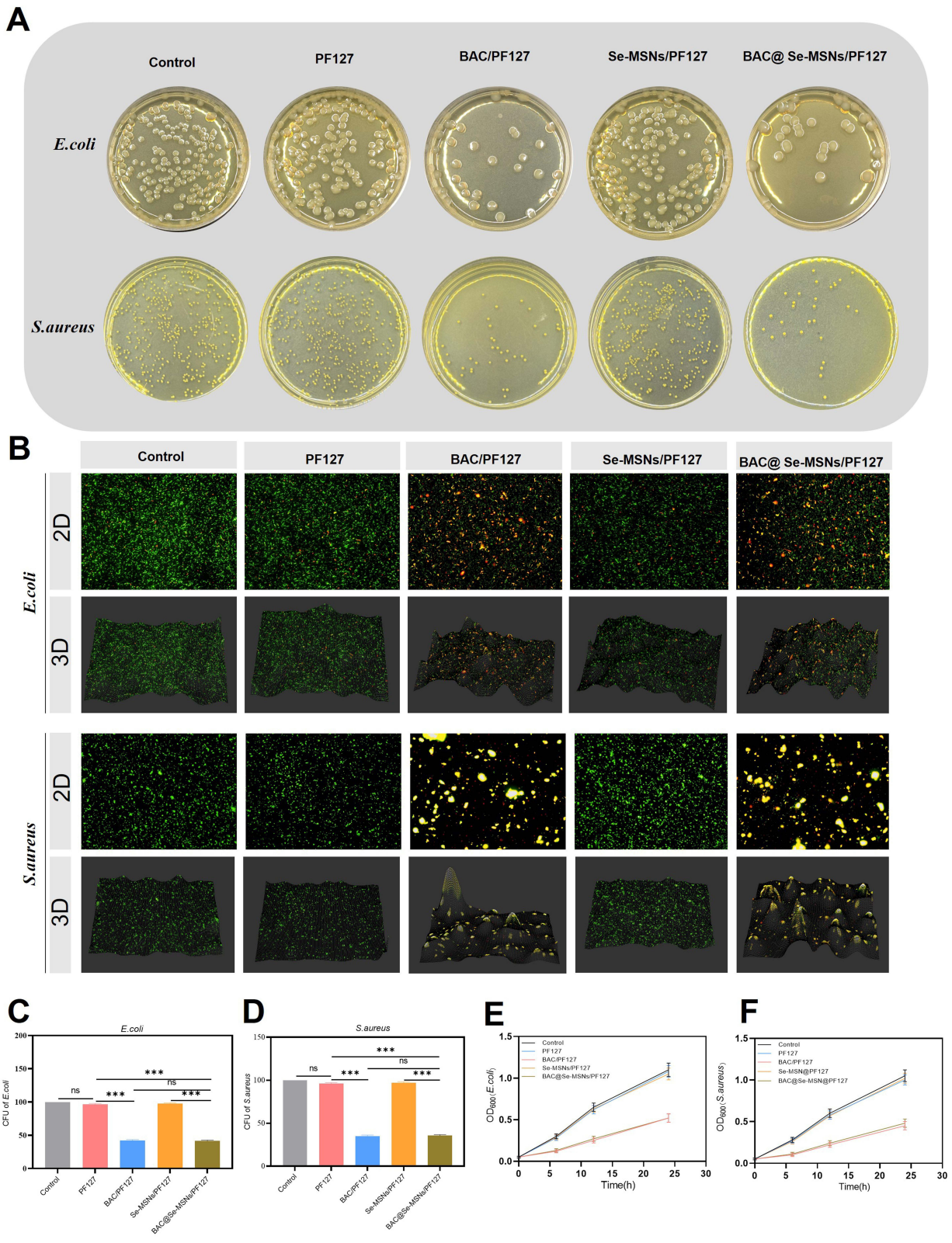

Figure 5 Antibacterial activity of BAC@Se-MSNs/PF127 hydrogel. (**A**) Plate culture of *E. coli* and *S. aureus* under different treatments. (**B**) 2D and 3D Live/Dead bacterial staining (green: live; red: dead). (**C**) Colony-forming unit (CFU) quantification for *E. coli*. (**D**) Colony-forming unit (CFU) quantification for *S. aureus*. (**E**) Growth curves of *E. coli* under different treatments. (**F**) Growth curves of *S. aureus* under different treatments. Data are mean ± SD (n = 3); ***P < 0.001, ns, not significant.

https://doi.org/10.2147/IJN.S594500

strong red fluorescence (dead cells) and greatly diminished green signals after exposure to BAC-loaded hydrogels (Figure 5B). Reconstruction analyses further revealed reduced adhesion and diminished biofilm organization.

CFU quantification confirmed significantly reduced bacterial counts in the BAC/PF127 and BAC@Se-MSNs/PF127 groups (Figure 5C and D, $P < 0.001$). Growth-curve assays showed markedly suppressed OD_{600} increases in both strains treated with BAC-containing systems, demonstrating effective inhibition of bacterial proliferation (Figure 5E and F). The antibacterial activity of BAC mainly contributes to reducing microbial burden and preventing local infection, while literature suggests that at the concentrations used, cationic surfactants do not significantly interfere with the redox activity or anti-inflammatory function of selenium within the composite system.[43,44]

BAC@Se-MSNs Composite Thermosensitive Hydrogel Accelerates Wound Healing in Diabetic Mice

To evaluate the therapeutic performance of BAC@Se-MSNs/PF127 in vivo, a streptozotocin-induced diabetic full-thickness skin wound model was established (Figure 6A). Mice were administered Control, PF127, BAC@PF127, Se-MSNs@PF127, or the combined BAC@Se-MSNs/PF127 hydrogel, and wound regeneration was tracked by serial imaging and area quantification (Figure 6B and C).

By day 7, wounds treated with the composite hydrogel exhibited more than 60% reduction in size and nearly complete closure by day 14, with only minimal crusting remaining. In contrast, the Control and PF127 groups showed pronounced inflammatory exudate and delayed contraction. BAC@PF127 and Se-MSNs@PF127 each produced moderate improvement, but neither matched the robust healing observed with the dual-functional composite. Statistical analysis confirmed substantially higher wound closure rates in the BAC@Se-MSNs/PF127 group at days 7, 10, and 14 ($P < 0.001$). These findings indicate a strong synergistic effect between BAC and Se-MSNs within the thermogelling matrix, markedly promoting wound repair in diabetic conditions.

Body weight trends over 14 days (Figure S3) suggested no systemic toxicity; all groups displayed slight reductions early after surgery, followed by progressive recovery. Mice receiving BAC@Se-MSNs/PF127 reached approximately 108% of baseline weight, reflecting good physiological tolerance. Pain scoring using the Mouse Grimace Scale (Figure S4) demonstrated a consistent decline across all groups from days 2–3, with BAC@Se-MSNs/PF127 showing the sharpest reduction ($P < 0.05$), suggesting alleviation of wound-associated discomfort.

BAC@Se-MSNs/PF127 Hydrogel Promotes Macrophage Polarization from Pro-Inflammatory M1 to Reparative M2 Phenotype

Macrophages orchestrate the inflammatory-to-repair transition in wound healing. Under diabetic conditions, however, sustained M1 activation and impaired switch to M2 macrophages hinder tissue recovery.[45,46] Selenium has been linked to enhanced macrophage polarization, including activation of the CSF-1–M2 axis and dampening of IL-6-mediated inflammatory injury [10]. To examine whether the composite hydrogel reshapes macrophage behavior in vivo, wound tissues were stained for CD68 (pan-macrophages), iNOS (M1), and CD206 (M2). On day 3, all groups contained abundant $CD68^+/iNOS^+$ cells, indicative of active inflammation, yet BAC@Se-MSNs/PF127 showed noticeably fewer M1 macrophages than other treatments. By day 7, a marked decline in M1 cells and an increase in $CD68^+/CD206^+$ cells were observed, with the composite hydrogel producing the most pronounced shift (Figure 7A and B).

Quantification confirmed that BAC@Se-MSNs/PF127 significantly decreased M1 proportions and elevated M2 fractions relative to Control and single-component hydrogels ($P < 0.001$, Figure 7C and D). These results demonstrate that the multifunctional hydrogel effectively alleviates excessive inflammation and promotes reparative macrophage polarization, facilitating earlier progression into the tissue-regeneration phase.

BAC@Se-MSNs/PF127 Hydrogel Enhances Tissue Regeneration and Angiogenesis in Diabetic Wounds

On day 14, regenerated tissues were collected to assess histological recovery. H&E staining revealed incomplete epithelial continuity and persistent gaps in the Control and PF127 groups. BAC@PF127 and Se-MSNs@PF127

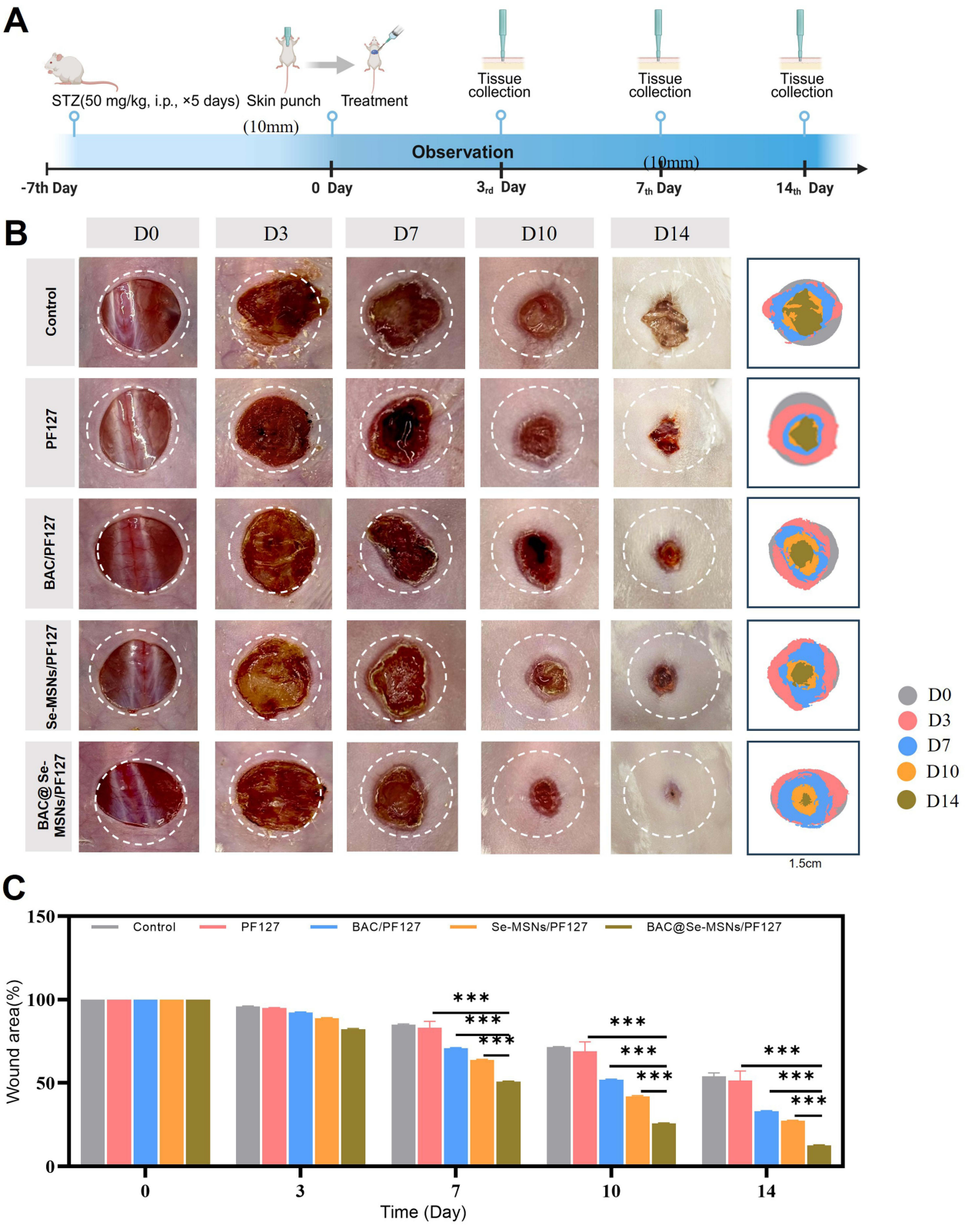

Figure 6 BAC@Se-MSNs/PF127 hydrogel accelerates wound healing in diabetic mice. (**A**) Schematic of diabetic wound model and treatment protocol. (**B**) Representative wound images and wound area changes at days 0, 3, 7, 10, and 14. (**C**) Quantitative analysis of wound area over time. Data are mean ± SD (n = 5); ***P < 0.001, ns, not significant. Scale bar = 1.5 cm.

https://doi.org/10.2147/IJN.S594500

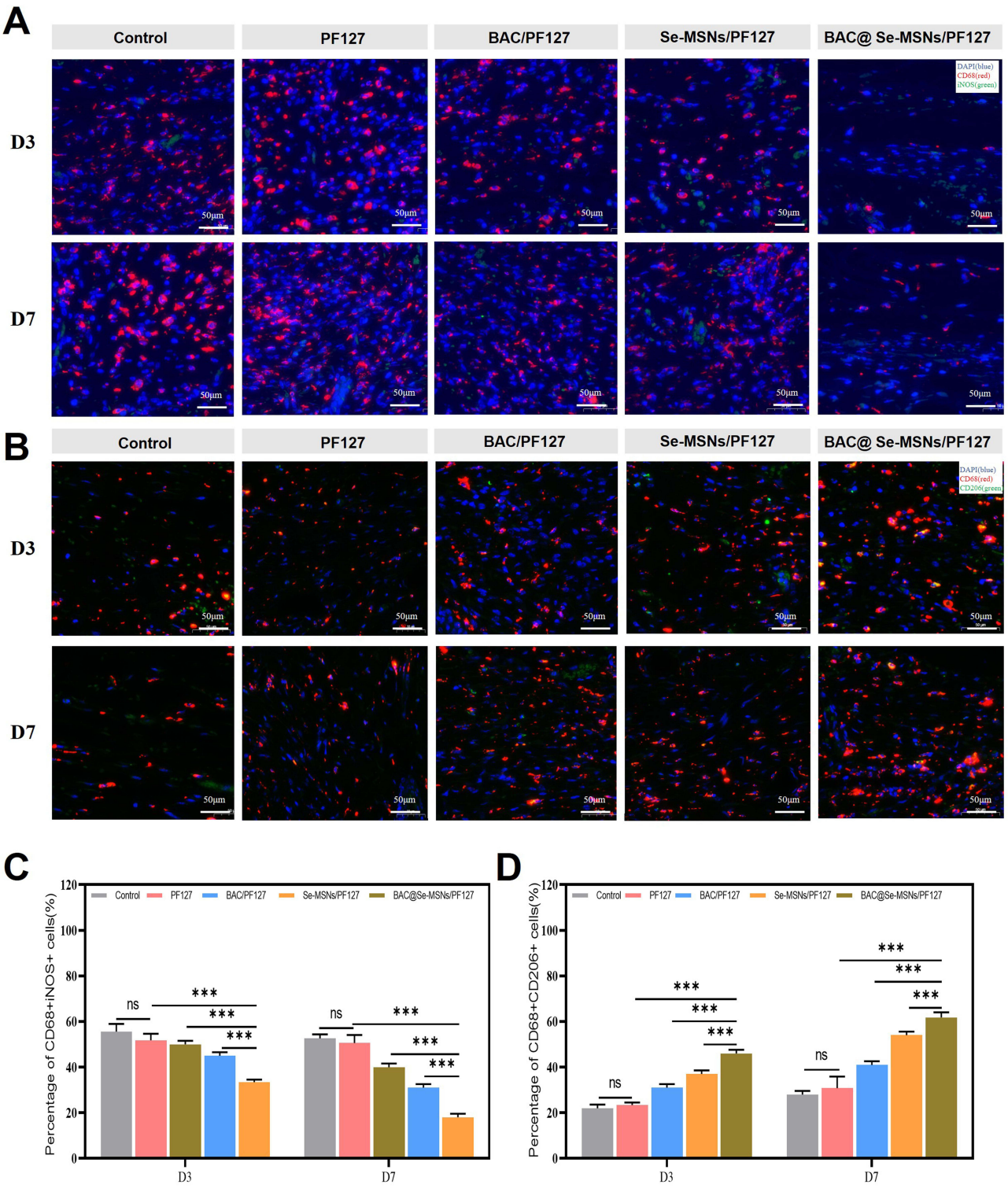

Figure 7 BAC@Se-MSNs/PF127 hydrogel modulates macrophage polarization in diabetic wounds. (**A**) Immunofluorescence showing M1 macrophages ($CD68^+/iNOS^+$, red/green, DAPI-stained nuclei in blue) at days 3 and 7. (**B**) Immunofluorescence showing M2 macrophages ($CD68^+/CD206^+$, red/green, DAPI-stained nuclei in blue). Scale bar = 50 μm. (**C**) Quantitative analysis of M1 ($CD68^+/iNOS^+$) macrophage proportions in wound tissues. (**D**) Quantitative analysis of M2 ($CD68^+/CD206^+$) macrophage proportions in wound tissues. Data are mean ± SD (n = 3); ***P < 0.001, ns, not significant.

https://doi.org/10.2147/IJN.S594500

provided partial enhancement, whereas the composite BAC@Se-MSNs/PF127 hydrogel yielded a fully stratified epidermis, dense dermal tissue, and emerging hair-follicle-like structures—hallmarks of advanced tissue reconstruction (Figure 8A).

Masson's trichrome staining indicated extensive and uniformly aligned collagen fibers in the composite hydrogel group, supporting accelerated matrix deposition and remodeling (Figure 8B). Immunohistochemical analysis showed the highest CD31 expression and a substantial increase in Ki67-positive cells in BAC@Se-MSNs/PF127-treated tissues (Figure 8C). Quantitative analyses confirmed significantly enhanced neovascularization and cell proliferation compared with Control and other treatment groups ($P < 0.01$, Figure 8D–F). Overall, these findings illustrate that the composite hydrogel promotes robust epithelial repair, collagen maturation, and vascular regeneration.

BAC@Se-MSNs/PF127 Hydrogel Facilitates Wound Repair via Modulation of Inflammation and Oxidative Stress–Related Pathways

To elucidate molecular mechanisms underlying the improved healing outcomes, RNA-seq analysis was performed on wound tissues. Differential expression analysis identified extensive transcriptomic remodeling, with 2260 genes upregulated and 2538 genes downregulated after BAC@Se-MSNs/PF127 treatment (Figure 9A). Heatmap visualization highlighted reduced expression of inflammation-related (Chil3, Krt6a, Slpi) and barrier-dysfunction genes, alongside elevated expression of genes promoting angiogenesis, proliferation, and matrix remodeling (Shh, Mc1r, Adamts18) (Figure 9B).

GO enrichment suggested significant involvement of leukocyte regulation, inflammatory response, extracellular matrix organization, and oxidation–reduction biological processes (Figure 9C). KEGG analysis revealed enrichment in cytokine–receptor interaction, chemokine signaling, actin cytoskeleton regulation, and oxidative phosphorylation (Figure 9D). GSEA further demonstrated activation of defense-response pathways, suppression of cytokine-binding signatures, and enhancement of NADPH-related oxidoreductase activity (Figure 9E–G). Collectively, these transcriptomic changes indicate that the hydrogel improves diabetic wound repair by mitigating excessive inflammation and enhancing mitochondrial metabolic activity and redox balance.

In vivo Biosafety Assessment of BAC@Se-MSNs/PF127 Hydrogel

Biosafety was assessed via hematological parameters, serum biochemistry, and histopathology. None of the measured blood indices (WBC, RBC, HGB, HCT, MCV, MCH, MCHC, PLT, RDW-SD, MPV) showed significant deviations from the Control group ($P > 0.05$, Figure S5). Liver (ALT, AST, ALP) and kidney (CREZ, UREA) function markers remained within normal ranges.

H&E staining of major organs—including heart, liver, spleen, lung, and kidney—displayed intact architecture with no evidence of inflammatory infiltration or structural abnormalities (Figure S6). Tissues from BAC@Se-MSNs/PF127-treated mice closely resembled those of the Control and PF127 groups, confirming favorable systemic biocompatibility. These results demonstrate that the composite hydrogel exerts no detectable systemic toxicity and is safe for in vivo application.

Conclusion

In conclusion, we developed a multifunctional composite hydrogel (BAC@Se-MSNs/PF127) for diabetic chronic wound treatment. By integrating benzalkonium chloride with selenium-doped mesoporous silica nanoparticles, the system simultaneously provides antibacterial, antioxidant, and immunomodulatory effects, thereby improving the wound microenvironment. The hydrogel demonstrated favorable injectability, sustained release behavior, and promoted endothelial migration and angiogenesis in vitro, as well as accelerated wound closure and tissue regeneration in diabetic mice. Mechanistically, these effects are associated with coordinated regulation of inflammation and redox balance. Overall, this study offers a promising and practical strategy for the design of multifunctional biomaterials for chronic wound management.

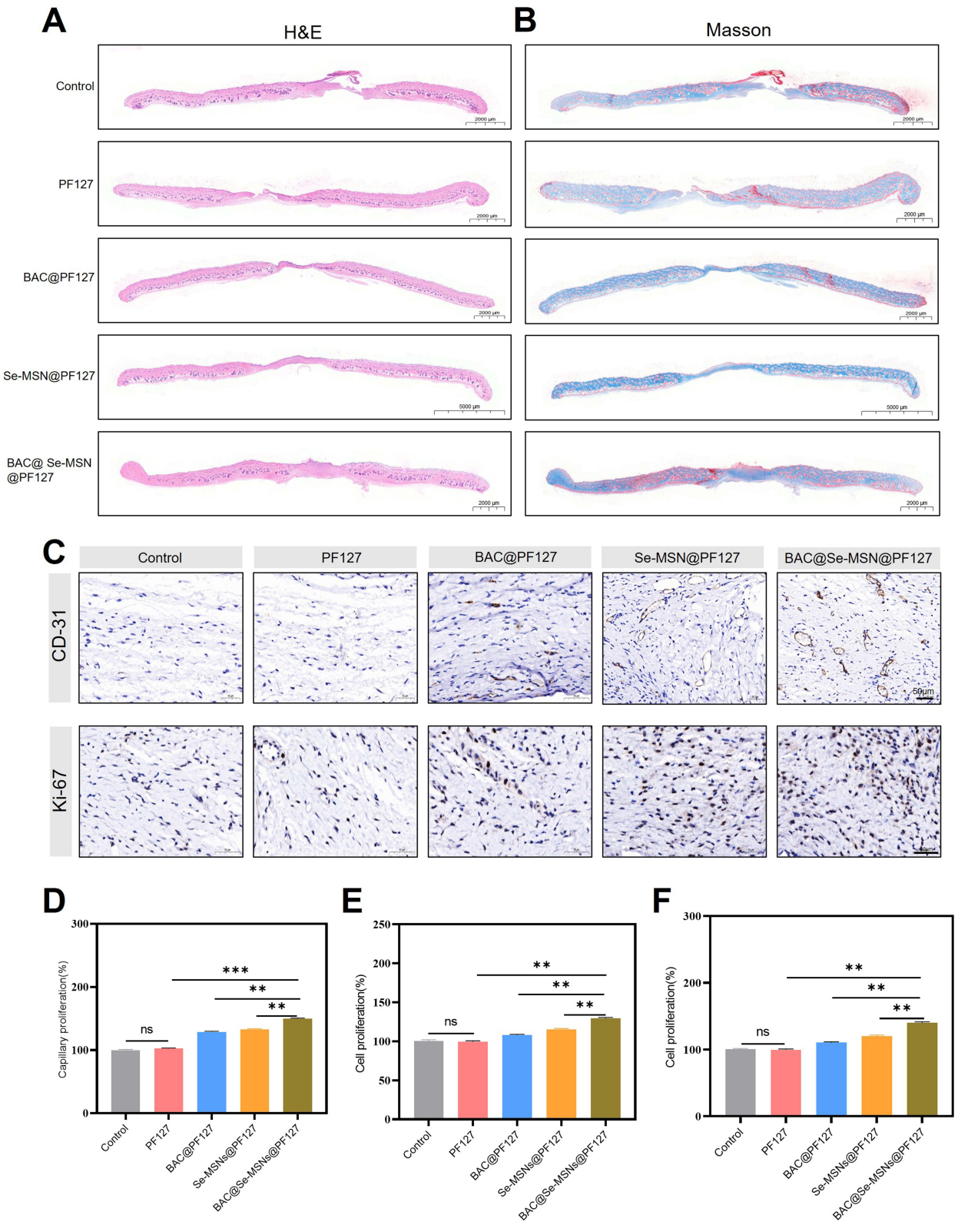

Figure 8 BAC@Se-MSNs/PF127 hydrogel promotes tissue regeneration and angiogenesis in diabetic wounds. (**A**) H&E staining showing wound tissue morphology at day 14. (**B**) Masson's trichrome staining showing collagen deposition and organization. (**C**) Immunohistochemistry for angiogenesis marker CD31 and proliferation marker Ki67. Scale bar = 50 μm. (**D**) Quantification of capillary density in wound dermis. (**E**) Quantification of epithelial cell proliferation rates. (**F**) Quantification of dermal cell proliferation rates. Data are mean ± SD (n = 3); **P < 0.01, ***P < 0.001, ns, not significant.

https://doi.org/10.2147/IJN.S594500

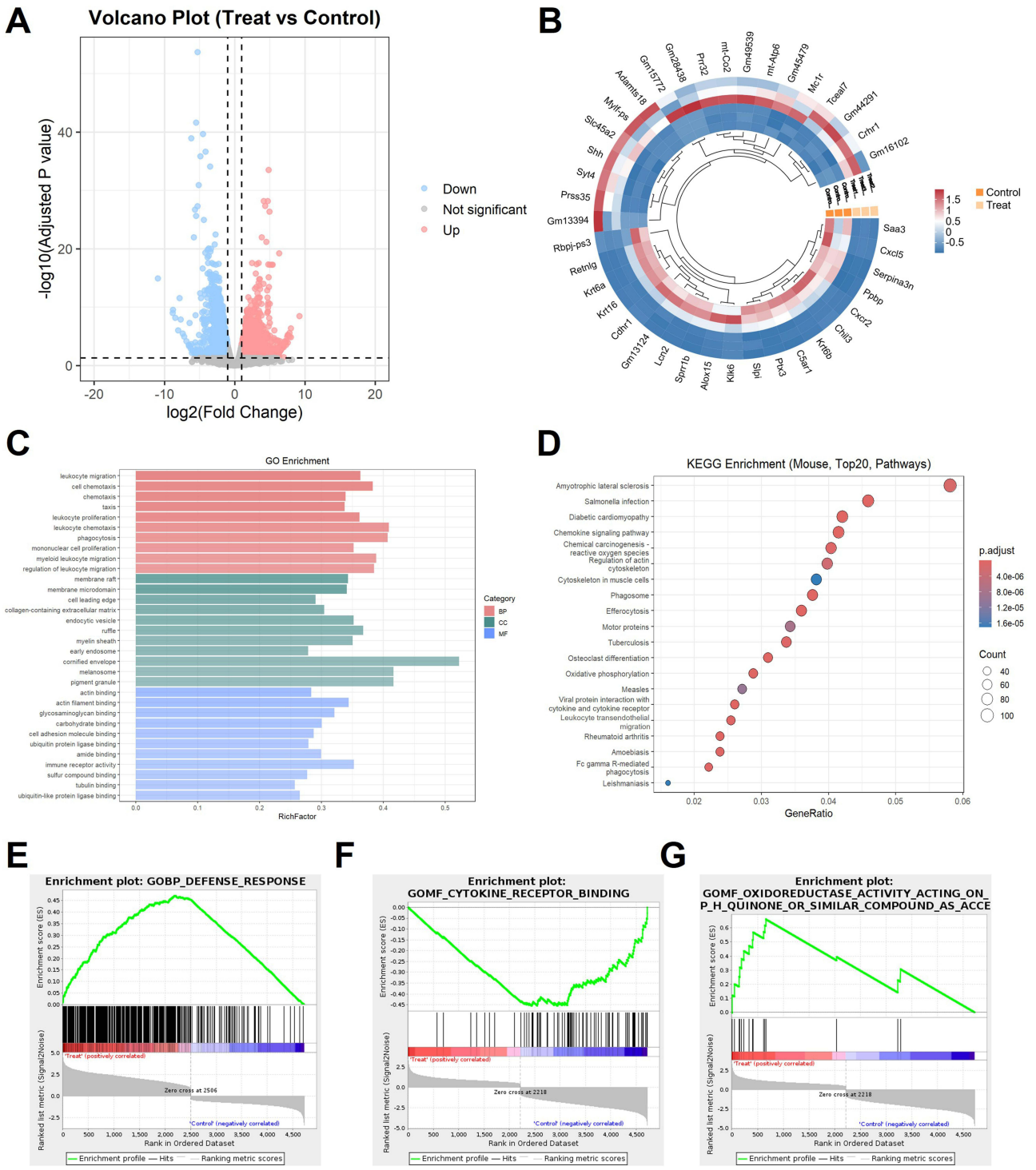

Figure 9 BAC@Se-MSNs/PF127 composite hydrogel modulates gene expression profiles and signaling pathways in diabetic wounds. (**A**) Volcano plot showing differentially expressed genes between the treated (BAC@Se-MSNs/PF127) and untreated control groups, with 2260 genes upregulated and 2538 genes downregulated ($|\log_2 FC| > 1$, $p < 0.05$). (**B**) Heatmap illustrating representative gene expression changes between the treated and control groups. (**C**) Gene Ontology (GO) enrichment analysis indicates that the differentially expressed genes are primarily involved in inflammatory response, cell migration, and redox processes. (**D**) KEGG pathway enrichment analysis reveals significant enrichment in pathways associated with cytokine signaling, cytoskeleton regulation, and oxidative phosphorylation. (**E**–**G**) Gene Set Enrichment Analysis (GSEA) demonstrates that the defense response pathway is activated (**E**), the cytokine receptor binding pathway is suppressed (**F**), and the oxidoreductase activity acting on the NADPH pathway is activated (**G**).

https://doi.org/10.2147/IJN.S594500

Data Sharing Statement

The data that support the findings of this study are available from the corresponding author upon reasonable request. All relevant data generated or analyzed during this study are included in this published article and its supplementary information files.

Ethics Approval and Consent to Participate

Animals were anesthetized with pentobarbital sodium (50 mg/kg, intraperitoneal injection) prior to all surgical procedures. At the conclusion of the experiments, animals were euthanized by an overdose of pentobarbital sodium (≥150 mg/kg, intraperitoneal injection). All animal procedures were performed in accordance with the Guidelines for the Care and Use of Laboratory Animals of China. The study was approved by the Institutional Animal Care and Use Committee of Tongji Hospital, Huazhong University of Science and Technology (approval number: T1-202505014, Wuhan, China). All efforts were made to minimize animal suffering.

Consent for Publication

No individual personal data is included in the study.

Acknowledgments

Yukun Liu and Kang Wang contributed equally to this work and are co-first authors.

Funding

This study was supported by grants from the National Natural Science Foundation of China (No. 82002101, 82002096).

Disclosure

The authors declare that they have no competing interests in this work.

References

1. McDermott K, Fang M, Boulton AJM, Selvin E, Etiology HCW. Epidemiology, and disparities in the burden of diabetic foot ulcers. *Diabetes Care*. 2023;46(1):209–221. doi:10.2337/dci22-0043
2. Mlynarska E, Czarnik W, Dzieza N, et al. Type 2 diabetes mellitus: new pathogenetic mechanisms, treatment and the most important complications. *Int J Mol Sci*. 2025;26(3). doi:10.3390/ijms26031094
3. Deng H, Li B, Shen Q, et al. Mechanisms of diabetic foot ulceration: a review. *J Diabetes*. 2023;15(4):299–312. doi:10.1111/1753-0407.13372
4. Dixon D, Edmonds M. Managing diabetic foot ulcers: pharmacotherapy for wound healing. *Drugs*. 2021;81(1):29–56. doi:10.1007/s40265-020-01415-8
5. Raja JM, Maturana MA, Kayali S, Khouzam A, Efeovbokhan N. Diabetic foot ulcer: a comprehensive review of pathophysiology and management modalities. *World J Clin Cases*. 2023;11(8):1684–1693. doi:10.12998/wjcc.v11.i8.1684
6. Miklosz A, Chabowski A. Adipose-derived mesenchymal stem cells therapy as a new treatment option for diabetes mellitus. *J Clin Endocrinol Metab*. 2023;108(8):1889–1897. doi:10.1210/clinem/dgad142
7. Li D, Wu N. Mechanism and application of exosomes in the wound healing process in diabetes mellitus. *Diabet Res Clin Pract*. 2022;187:109882. doi:10.1016/j.diabres.2022.109882
8. Wang Q, Liu C, An J, Liu J, Wang Y, Cai Y. Mechanisms of microbial infection and wound healing in diabetic foot ulcer: pathogenicity in the inflammatory-proliferative phase, chronicity, and treatment strategies. *Front Endocrinol*. 2025;16:1657928. doi:10.3389/fendo.2025.1657928
9. Jiang P, Li Q, Luo Y, et al. Current status and progress in research on dressing management for diabetic foot ulcer. *Front Endocrinol*. 2023;14:1221705. doi:10.3389/fendo.2023.1221705
10. Polk C, Sampson MM, Roshdy D, Davidson LE. Skin and soft tissue infections in patients with diabetes mellitus. *Infect Dis Clin North Am*. 2021;35(1):183–197. doi:10.1016/j.idc.2020.10.007
11. Guo Q, Ying G, Jing O, et al. Influencing factors for the recurrence of diabetic foot ulcers: a meta-analysis. *Int Wound J*. 2023;20(5):1762–1775. doi:10.1111/iwj.14017
12. Ghotaslou R, Memar MY, Alizadeh N. Classification, microbiology and treatment of diabetic foot infections. *J Wound Care*. 2018;27(7):434–441. doi:10.12968/jowc.2018.27.7.434
13. Chang M, Nguyen TT. Strategy for treatment of infected diabetic foot ulcers. *Acc Chem Res*. 2021;54(5):1080–1093. doi:10.1021/acs.accounts.0c00864
14. Sen CK, Roy S, Mathew-Steiner SS, Gordillo GM. Biofilm management in wound care. *Plast Reconstr Surg*. 2021;148(2):275e–288e. doi:10.1097/PRS.0000000000008142
15. Goswami AG, Basu S, Banerjee T, Shukla VK. Biofilm and wound healing: from bench to bedside. *Eur J Med Res*. 2023;28(1):157. doi:10.1186/s40001-023-01121-7

16. Arias-Moliz MT, Ruiz-Linares M, Cassar G, et al. The effect of benzalkonium chloride additions to AH Plus sealer. Antimicrobial, physical and chemical properties. *J Dent*. 2015;43(7):846–854. doi:10.1016/j.jdent.2015.05.003
17. Pirani F, Eshghi H, Rounaghi SA. Immobilized Cu(0) nanoparticles on montmorillonite-modified with benzalkonium chloride (MMT-BAC@Cu (0)): as an eco-friendly and proficient heterogeneous nano-catalyst for green synthesis of 5-substituted 1H-tetrazoles. *RSC Adv*. 2023;13 (9):6160–6170. doi:10.1039/d2ra08208j
18. Hossain SI, Bajrami D, Altun N, et al. Development of super nanoantimicrobials combining AgCl, tetracycline and benzalkonium chloride. *Discov Nano*. 2024;19(1):100. doi:10.1186/s11671-024-04043-3
19. Gholamrezazadeh M, Shakibaie MR, Monirzadeh F, Masoumi S, Hashemizadeh Z. Effect of nano-silver, nano-copper, deconex and benzalkonium chloride on biofilm formation and expression of transcription regulatory quorum sensing gene (rh1R) in drug-resistance Pseudomonas aeruginosa burn isolates. *Burns*. 2018;44(3):700–708. doi:10.1016/j.burns.2017.10.021
20. Zare H, Rezayi M, Aryan E, et al. Nanotechnology-driven advances in the treatment of diabetic wounds. *Biotechnol Appl Biochem*. 2021;68 (6):1281–1306. doi:10.1002/bab.2051
21. Smith RA. Nanotechnology in the future treatment of diabetic wounds. *Rev Diabet Stud*. 2020;16(1):1–12. doi:10.1900/RDS.2020.16.1
22. Zhao X, Xu Z, Wang D, et al. Silicon-based nanomaterials in chronic wound healing: mechanisms, therapeutic applications, and clinical prospects. *Int J Nanomed*. 2025;20:11959–11988. doi:10.2147/IJN.S528531
23. Heidari R, Assadollahi V, Shakib Manesh MH, Mirzaei SA, Elahian F. Recent advances in mesoporous silica nanoparticles formulations and drug delivery for wound healing. *Int J Pharm*. 2024;665:124654. doi:10.1016/j.ijpharm.2024.124654
24. Chen L, Zhou X, He C. Mesoporous silica nanoparticles for tissue-engineering applications. *Wiley Interdiscip Rev Nanomed Nanobiotechnol*. 2019;11(6):e1573. doi:10.1002/wnan.1573
25. Mojadadi A, Au A, Salah W, Witting P, Ahmad G. Role for selenium in metabolic homeostasis and human reproduction. *Nutrients*. 2021;13(9). doi:10.3390/nu13093256
26. Xiao X, Deng H, Lin X, et al. Selenium nanoparticles: properties, preparation methods, and therapeutic applications. *Chem Biol Interact*. 2023;378:110483. doi:10.1016/j.cbi.2023.110483
27. Gao S, Tuda M. Silica and selenium nanoparticles attract or repel scale insects by altering physicochemical leaf traits. *Plants*. 2024;13(7). doi:10.3390/plants13070952
28. Amin RS, Fetohi AE, Khater DZ, et al. Selenium-transition metal supported on a mixture of reduced graphene oxide and silica template for water splitting. *RSC Adv*. 2023;13(23):15856–15871. doi:10.1039/d3ra01945d
29. Chen X, Song H, Song K, et al. Temperature-sensitive hydrogel releasing pectolinarin facilitate scarless wound healing. *J Cell Mol Med*. 2024;28 (4):e18130. doi:10.1111/jcmm.18130
30. Liu Y, Gao F, Liu S, et al. A smart CO-releasing MnSiO(3)-based hydrogel enhances diabetic wound healing through NIR-triggered antibacterial, anti-inflammatory, and pro-regenerative mechanisms. *Mater Today Bio*. 2025;34:102084. doi:10.1016/j.mtbio.2025.102084
31. Li H, Wen H, Zhang H, et al. A multifunctional dihydromyricetin-loaded hydrogel for the sequential modulation of diabetic wound healing and glycemic control. *Burns Trauma*. 2025;13:tkaf024. doi:10.1093/burnst/tkaf024
32. Chen J, Chen D, Chen J, et al. An all-in-one CO gas therapy-based hydrogel dressing with sustained insulin release, anti-oxidative stress, antibacterial, and anti-inflammatory capabilities for infected diabetic wounds. *Acta Biomater*. 2022;146:49–65. doi:10.1016/j.actbio.2022.04.043
33. Liu Y, Wang K, Tang T, et al. Rosuvastatin-loaded nanocomposite hydrogel accelerates diabetic wound healing by coordinating multimodal regeneration. *Chem Eng J*. 2026;527:171620. doi:10.1016/j.cej.2025.171620
34. Deng L, Du C, Song P, et al. The role of oxidative stress and antioxidants in diabetic wound healing. *Oxid Med Cell Longev*. 2021;2021:8852759. doi:10.1155/2021/8852759
35. Zhao H, Huang J, Li Y, et al. ROS-scavenging hydrogel to promote healing of bacteria infected diabetic wounds. *Biomaterials*. 2020;258:120286. doi:10.1016/j.biomaterials.2020.120286
36. Dunnill C, Patton T, Brennan J, et al. Reactive oxygen species (ROS) and wound healing: the functional role of ROS and emerging ROS-modulating technologies for augmentation of the healing process. *Int Wound J*. 2017;14(1):89–96. doi:10.1111/iwj.12557
37. Jain A, Kolipaka T, Pandey G, et al. Innovative approaches to diabetic wound healing: focusing on ros and redox signals. *Mol Pharm*. 2025;22 (10):5738–5766. doi:10.1021/acs.molpharmaceut.5c00491
38. Heo JS. Selenium-stimulated exosomes enhance wound healing by modulating inflammation and angiogenesis. *Int J Mol Sci*. 2022;23(19). doi:10.3390/ijms231911543
39. Okonkwo UA, DiPietro LA. Diabetes and wound angiogenesis. *Int J Mol Sci*. 2017;18(7). doi:10.3390/ijms18071419
40. Ahmed W, Li S, Liang M, Kang Y, Liu X, Gao C. Multifunctional drug- and AuNRs-loaded ROS-responsive selenium-containing polyurethane nanofibers for smart wound healing. *ACS Biomater Sci Eng*. 2024;10(6):3946–3957. doi:10.1021/acsbiomaterials.4c00363
41. Rodriguez-Rodriguez N, Martinez-Jimenez I, Garcia-Ojalvo A, et al. Wound chronicity, impaired immunity and infection in diabetic patients. *MEDICC Rev*. 2022;24(1):44–58. doi:10.37757/MR2021.V23.N3.8
42. Zhang M, Feng J, Zhong Y, et al. In-situ synthesis of drug-containing bactericidal rough silica nanoparticles for antibacterial coating. *Chem Eng J*. 2022;440:135837.
43. Cosin-Tomas M, Senserrich J, Arumi-Planas M, et al. Role of resveratrol and selenium on oxidative stress and expression of antioxidant and anti-aging genes in immortalized lymphocytes from alzheimer's disease patients. *Nutrients*. 2019;11(8). doi:10.3390/nu11081764
44. Sak M, Al-Faiyz YS, Elsawy H, Shaaban S. Novel organoselenium redox modulators with potential anticancer, antimicrobial, and antioxidant activities. *Antioxidants*. 2022;11(7). doi:10.3390/antiox11071231
45. Wolf SJ, Melvin WJ, Gallagher K. Macrophage-mediated inflammation in diabetic wound repair. *Semin Cell Dev Biol*. 2021;119:111–118. doi:10.1016/j.semcdb.2021.06.013
46. Sharifiaghdam M, Shaabani E, Faridi-Majidi R, De Smedt SC, Braeckmans K, Fraire JC. Macrophages as a therapeutic target to promote diabetic wound healing. *Mol Ther*. 2022;30(9):2891–2908. doi:10.1016/j.ymthe.2022.07.016